

Dynamics and thermalization in correlated one-dimensional lattice systems

Marcos Rigol*

Department of Physics, Georgetown University,
Washington, DC 20057, USA

Abstract

We review exact approaches and recent results related to the relaxation dynamics and description after relaxation of various one-dimensional lattice systems of hard-core bosons after a sudden quench. We first analyze the integrable case, where the combination of analytical insights and computational techniques enable one to study large system sizes. Thermalization does not occur in this regime. However, after relaxation, observables can be described by a generalization of the Gibbs ensemble. We then utilize full exact diagonalization to study what happens as integrability is broken. We show that thermalization does occur in finite nonintegrable systems provided they are sufficiently far away from the integrable point. We argue that the onset of thermalization can be understood in terms of the eigenstate thermalization hypothesis.

1 Introduction

Understanding how statistical properties emerge from microscopic models of many-particle systems is of fundamental interest in several fields in physics. This topic has been extensively studied in the context of classical systems. We know that if we perturb a generic isolated gas in many different ways, it will still relax to

*Present address: Department of Physics, The Pennsylvania State University, University Park, Pennsylvania 16802, USA

a unique (Maxwell) velocity distribution determined by its energy. This universal behavior (thermalization) has been understood in terms of dynamical chaos, namely, the nonlinear equations that drive the dynamics ensure that the system explores ergodically all the available phase space [1]. However, there is a class of models, known as integrable models, for which the presence of a full set of conserved quantities precludes thermalization. In this case, dictated by the initial conditions, the dynamics is restricted to a limited region of phase space. More than fifty years ago, Fermi, Pasta, and Ulam (FPU) [2] set up one of the first numerical experiments to study how thermalization takes place in a one-dimensional (1d) lattice of harmonic oscillators once nonlinear couplings were added. No signs of ergodicity were found. Those unexpected results led to intensive research [3] and ultimately to the development of modern chaos theory [4].

Recent advances in cooling and trapping atomic gases has led to increased interest in understanding what happens in the quantum case. In those experiments, the high degree of isolation, combined with the possibility of controlling interactions and the effective dimensionality of the gas, has allowed experimentalists to realize [5, 6, 7] and explore the dynamics [8, 9] of nearly integrable 1d systems. Thermalization was not observed in one of the experiments [8] but was indirectly confirmed in the other [9]. These results have motivated intense theoretical research on the dynamics and thermalization of isolated quantum systems after a sudden quench, both in the integrable [10, 11, 12, 13, 14, 15, 16, 17, 18, 19, 20, 21, 22, 23] and nonintegrable [24, 25, 26, 27, 28, 29, 30, 31, 32, 33, 34, 35, 36, 37] regimes.

Here, we review results for 1d systems of hard-core bosons (HCBs) on a lattice. We show that thermalization does not occur (in general) when the system is integrable. However, observables after relaxation can be described by a generalization of the Gibbs ensemble [10, 12, 23]. As integrability is broken, thermalization does take place [31, 32, 37], and is shown to follow after the eigenstate thermalization hypothesis [26, 38, 39].

2 Methodology

The HCB Hamiltonian of interest reads

$$\begin{aligned} \hat{H}_{\text{HCB}} = & \sum_{j=1}^L \left[-J (\hat{b}_j^\dagger \hat{b}_{j+1} + \text{H.c.}) + V \left(\hat{n}_j - \frac{1}{2} \right) \left(\hat{n}_{j+1} - \frac{1}{2} \right) \right] + \sum_{j=1}^L V_j^{\text{ext}} \hat{n}_j \\ & + \sum_{j=1}^L \left[-J' (\hat{b}_j^\dagger \hat{b}_{j+2} + \text{H.c.}) + V' \left(\hat{n}_j - \frac{1}{2} \right) \left(\hat{n}_{j+2} - \frac{1}{2} \right) \right], \end{aligned} \quad (1)$$

where J (J') is the nearest (next-nearest) neighbor hopping, V (V') is the nearest (next-nearest) neighbor interaction, and V_j^{ext} is an external potential. The HCB creation (annihilation) operator in each site is denoted by \hat{b}_j^\dagger (\hat{b}_j), the site number occupation by $\hat{n}_j = \hat{b}_j^\dagger \hat{b}_j$, and $\hat{b}_{L+1} \equiv \hat{b}_1$ and $\hat{b}_{L+2} \equiv \hat{b}_2$ for periodic systems. Since HCBs are bosons for which the on-site repulsion is infinite, in addition to the standard commutation relations for bosons, their creation and annihilation operators satisfy the constraints $\hat{b}_j^{\dagger 2} = \hat{b}_j^2 = 0$, which preclude multiple occupancy of the lattice sites.

For $J' = V' = 0$, and any value of V , this model is integrable [40]. The approaches used to study this model are described below.

2.1 Integrable Case with $V = J' = V' = 0$

This problem can be exactly solved if one realizes that the HCB Hamiltonian can be mapped onto a spin Hamiltonian by means of the Holstein–Primakoff transformation [41],

$$\sigma_j^+ = \hat{b}_j^\dagger \sqrt{1 - \hat{b}_j^\dagger \hat{b}_j}, \quad \sigma_j^- = \sqrt{1 - \hat{b}_j^\dagger \hat{b}_j} \hat{b}_j, \quad \sigma_j^z = \hat{b}_j^\dagger \hat{b}_j - 1/2, \quad (2)$$

and that the spin Hamiltonian can be mapped onto a noninteracting fermion Hamiltonian utilizing the Jordan–Wigner transformation [42, 40]

$$\sigma_j^+ = \hat{f}_j^\dagger e^{-i\pi \sum_{k<j} \hat{f}_k^\dagger \hat{f}_k}, \quad \sigma_j^- = e^{i\pi \sum_{k<j} \hat{f}_k^\dagger \hat{f}_k} \hat{f}_j, \quad \sigma_j^z = \hat{f}_j^\dagger \hat{f}_j - 1/2. \quad (3)$$

For simplicity, we will assume open boundary conditions. The resulting Hamiltonian for the noninteracting fermions reads

$$\hat{H}_{\text{F}} = -J \sum_{j=1}^{L-1} (\hat{f}_j^\dagger \hat{f}_{j+1} + \text{H.c.}) + \sum_{j=1}^L V_j^{\text{ext}} \hat{f}_j^\dagger \hat{f}_j, \quad (4)$$

and, since it is quadratic, it can be easily diagonalized. Hence, HCBs and noninteracting fermions share the same spectrum. The density profiles and any density-density correlations will also coincide in both systems. The nontrivial differences between HCBs and noninteracting fermions are revealed by the off-diagonal correlations. In particular, we will be interested in the time evolution of the equal-time one-particle correlations $\hat{\rho}_{jk}$, needed to compute the momentum distribution function. Once again using Eq. (2), $\rho_{jk} \equiv \langle \hat{b}_j^\dagger \hat{b}_k \rangle = \langle \sigma_j^+ \sigma_k^- \rangle = \langle \sigma_k^- \sigma_j^+ + \delta_{jk}(1 - 2\sigma_j^- \sigma_j^+) \rangle$, and we focus on how to compute $G_{jk} = \langle \sigma_j^- \sigma_k^+ \rangle$. Using (3), $G_{jk}(t)$ can be written as [43, 44]

$$G_{jk}(t) = \langle \Psi_F(t) | \prod_{l=1}^{j-1} e^{i\pi \hat{f}_l^\dagger \hat{f}_l} \hat{f}_j \hat{f}_k^\dagger \prod_{m=1}^{k-1} e^{-i\pi \hat{f}_m^\dagger \hat{f}_m} | \Psi_F(t) \rangle, \quad (5)$$

where $|\Psi_F(t)\rangle = e^{-i\hat{H}_F t/\hbar} |\Psi_F^I\rangle$, $|\Psi_F^I\rangle = \prod_{n=1}^N \sum_{q=1}^L P_{qn}^I \hat{f}_q^\dagger |0\rangle$ is the initial state (a Slater determinant), N is the number of particles, and t the time. The action of exponentials whose exponents are bilinear in fermionic creation and annihilation operators (such as \hat{H}_F) on Slater determinants generates new Slater determinants, so $|\Psi_F(t)\rangle = \prod_{n=1}^N \sum_{q=1}^L P_{qn}(t) \hat{f}_q^\dagger |0\rangle$. The matrix $\mathbf{P}(t)$ can be computed as $\mathbf{P}(t) = e^{-i\mathbf{H}_F t/\hbar} \mathbf{P}^I = \mathbf{U} e^{-i\mathbf{E}t/\hbar} \mathbf{U}^\dagger \mathbf{P}^I$ (where \mathbf{H}_F is the corresponding matrix representation of \hat{H}_F), and we have used that $\mathbf{H}_F \mathbf{U} = \mathbf{U} \mathbf{E}$, where \mathbf{E} is a diagonal matrix containing the eigenenergies and \mathbf{U} is the unitary matrix of eigenvectors. Furthermore, the action of $\prod_{m=1}^{k-1} e^{-i\pi \hat{f}_m^\dagger \hat{f}_m}$ on $|\Psi_F(t)\rangle$ changes the sign of $P_{qn}(t)$ for $q \leq k-1$, $n = 1, \dots, N$, and the creation of a particle at site k implies the addition of a column with only one nonzero element [$P_{kN+1}(t) = 1$] [the same applies to the action of $\prod_{l=1}^{j-1} e^{i\pi \hat{f}_l^\dagger \hat{f}_l} \hat{f}_j$ on the left of Eq. (5)]. Hence,

$$G_{jk}(t) = \langle 0 | \prod_{n=1}^N \sum_{q=1}^L P_{qn}^{*j}(t) \hat{f}_q \prod_{l=1}^N \sum_{m=1}^L P_{ml}^k(t) \hat{f}_l^\dagger | 0 \rangle, \quad (6)$$

$$= \det \left\{ \left[\mathbf{P}^j(t) \right]^\dagger \mathbf{P}^k(t) \right\}. \quad (7)$$

In Eq. (6), the matrix elements $P_{qn}^j(t)$ and $P_{ml}^k(t)$ have the form

$$P_{\beta\gamma}^\alpha(t) = \begin{cases} -P_{\beta\gamma}(t) & \text{for } \beta < \alpha, \gamma = 1, \dots, N \\ P_{\beta\gamma}(t) & \text{for } \beta \geq \alpha, \gamma = 1, \dots, N \\ \delta_{\alpha\beta} & \text{for } \gamma = N+1 \end{cases}, \quad (8)$$

with $\alpha = j, k$, $\beta = q, m$, and $\gamma = n, l$. Equation (7) follows from (6) by using the identity

$$\langle 0 | \hat{f}_{\alpha_1} \cdots \hat{f}_{\alpha_{N+1}} \hat{f}_{\beta_{N+1}}^\dagger \cdots \hat{f}_{\beta_1}^\dagger | 0 \rangle = \epsilon^{\lambda_1 \cdots \lambda_{N+1}} \delta_{\alpha_1 \beta_{\lambda_1}} \cdots \delta_{\alpha_{N+1} \beta_{\lambda_{N+1}}}, \quad (9)$$

where $\epsilon^{\lambda_1 \dots \lambda_{N+1}}$ is the Levi-Civita symbol in $N + 1$ dimensions, and the indices λ have values between 1 and $N + 1$. Employing Eq. (7), ρ_{jk} can be calculated in polynomial time, scaling as $L^2 N^3$, using a computer.

We will also be interested in describing the momentum distribution function after relaxation by using statistical ensembles. A polynomial time approach in this case is only known to us within the grand-canonical formalism [45]. The one-particle density matrix in this ensemble can be written as

$$\begin{aligned} \rho_{jk} &\equiv \frac{1}{Z} \text{Tr} \left\{ \hat{b}_j^\dagger \hat{b}_k e^{-(\hat{H}_{\text{HCB}} - \mu \sum_n \hat{b}_n^\dagger \hat{b}_n)/k_B T} \right\} \\ &= \frac{1}{Z} \text{Tr} \left\{ \hat{f}_j^\dagger \hat{f}_k \prod_{l=1}^{k-1} e^{i\pi \hat{f}_l^\dagger \hat{f}_l} e^{-(\hat{H}_{\text{F}} - \mu \sum_n \hat{f}_n^\dagger \hat{f}_n)/k_B T} \prod_{l=1}^{j-1} e^{-i\pi \hat{f}_m^\dagger \hat{f}_m} \right\}, \end{aligned} \quad (10)$$

where μ is the chemical potential, k_B is Boltzmann's constant, T the temperature, and $Z = \text{Tr}\{e^{-(\hat{H}_{\text{HCB}} - \mu \sum_n \hat{b}_n^\dagger \hat{b}_n)/k_B T}\}$ (identical for HCBs and fermions) is the partition function. To arrive to Eq. (10), in addition to the Jordan–Wigner transformation [Eq. (3)], we have used the cyclic property of the trace. Another useful property of the trace, over the fermionic Fock space [45], is

$$\text{Tr} \left\{ e^{\sum_{jk} \hat{f}_j^\dagger X_{jk} \hat{f}_k} e^{\sum_{lm} \hat{f}_l^\dagger Y_{lm} \hat{f}_m} \dots e^{\sum_{nq} \hat{f}_n^\dagger Z_{nq} \hat{f}_q} \right\} = \det \left[\mathbf{I} + e^{\mathbf{X}} e^{\mathbf{Y}} \dots e^{\mathbf{Z}} \right], \quad (11)$$

where \mathbf{I} is the identity matrix. Equation (11) allows us to compute Z as $Z = \prod_j [1 + e^{-(E_{jj} - \mu)/k_B T}]$. By noticing that for $j \neq k$, we can write $\hat{f}_j^\dagger \hat{f}_k = \exp(\sum_{nq} \hat{f}_n^\dagger A_{nq} \hat{f}_q) - 1$, where the only nonzero element of \mathbf{A} is $A_{jk} = 1$, the off-diagonal elements of ρ_{jk} ($j \neq k$) can be obtained as

$$\begin{aligned} \rho_{jk} &= \frac{1}{Z} \left\{ \det \left[\mathbf{I} + (\mathbf{I} + \mathbf{A}) \mathbf{O}_1 \mathbf{U} e^{-(\mathbf{E} - \mu \mathbf{I})/k_B T} \mathbf{U}^\dagger \mathbf{O}_2 \right] \right. \\ &\quad \left. - \det \left[\mathbf{I} + \mathbf{O}_1 \mathbf{U} e^{-(\mathbf{E} - \mu \mathbf{I})/k_B T} \mathbf{U}^\dagger \mathbf{O}_2 \right] \right\}, \end{aligned} \quad (12)$$

where \mathbf{O}_1 (\mathbf{O}_2) is diagonal with the first $j-1$ ($k-1$) elements of the diagonal equal to -1 and the others equal to 1. The diagonal elements of ρ_{jk} are the same as for noninteracting fermions and can be computed as

$$\rho_{jj} = \left[\mathbf{I} + e^{-(\mathbf{H}_{\text{F}} - \mu \mathbf{I})/k_B T} \right]_{jj}^{-1} = \left[\mathbf{U} \left(\mathbf{I} + e^{-(\mathbf{E} - \mu \mathbf{I})/k_B T} \right)^{-1} \mathbf{U}^\dagger \right]_{jj}. \quad (13)$$

The computational time within this approach scales as L^5 .

The momentum distribution function $n(k)$ in and out of equilibrium, is then determined by the expression $n(k) = (1/L) \sum_{mn} e^{-ik(m-n)} \rho_{nm}$.

2.2 Nonintegrable Case with $V^{\text{ext}} = 0$

For this case, we make use of full exact diagonalization (see, e.g., [46]). This approach has the disadvantage that the dimension of the matrices needing to be diagonalized scales exponentially with system size. Since the Hamiltonian (1) conserves the total number of particles, we work with a fixed number of particles $N = L/3$, reducing the dimensionality of our problem from 2^L to $\binom{L}{N}$. To further reduce the dimensionality of the matrices to be diagonalized, we consider systems with periodic boundary conditions and no external potential ($V^{\text{ext}} = 0$). Then, by using translational symmetry, we can block-diagonalize the Hamiltonian, with the size of each momentum block being $\sim 1/L$ the size of the original matrix. All momentum sectors, the dimensions of which are shown in the table below [34], are diagonalized. They are all used to construct the microcanonical and canonical ensembles.

Dimension of all momentum sectors ($k = 2\pi\kappa/L$)				
$L = 18$	$\kappa = 0, 6$	$\kappa = 1, 5, 7$	$\kappa = 2, 4, 8$	$\kappa = 3, 9$
dimension	1038	1026	1035	1028
$L = 21$	$\kappa = 0, 7$	other κ 's		
dimension	5538	5537		
$L = 24$	$\kappa = 0, 8$	$\kappa = 4, 12$	$\kappa = 2, 6, 10$	odd κ 's
dimension	30667	30666	30664	30624

3 Results

We focus on the dynamics after a sudden quench. This means that we start with some eigenstate of an initial Hamiltonian, which may not be the ground state, then at $t = 0$ some parameter is changed and the system is allowed to evolve. Independently of whether the Hamiltonian is integrable or not, one can always write the initial state wavefunction $|\psi_{\text{ini}}\rangle$ in the eigenstate basis of the final Hamiltonian, i.e., $|\psi_{\text{ini}}\rangle = \sum_{\alpha} C_{\alpha} |\Psi_{\alpha}\rangle$ with $C_{\alpha} = \langle \Psi_{\alpha} | \psi_{\text{ini}} \rangle$ and $\hat{H} |\Psi_{\alpha}\rangle = E_{\alpha} |\Psi_{\alpha}\rangle$. The dynamics of the wave-function takes the form $|\psi(t)\rangle = e^{-i\hat{H}t/\hbar} |\psi_{\text{ini}}\rangle = \sum_{\alpha} e^{-iE_{\alpha}t/\hbar} C_{\alpha} |\Psi_{\alpha}\rangle$ and the expectation value of any observable \hat{O} can be written as $\langle \hat{O}(t) \rangle \equiv \langle \psi(t) | \hat{O} | \psi(t) \rangle = \sum_{\alpha, \beta} C_{\alpha}^* C_{\beta} e^{i(E_{\alpha} - E_{\beta})t/\hbar} O_{\alpha\beta}$, where $O_{\alpha\beta} = \langle \Psi_{\alpha} | \hat{O} | \Psi_{\beta} \rangle$. If the spectrum is nondegenerate, the infinite time average and the observable after relaxation is determined by

$$\overline{\langle \hat{O} \rangle} \equiv O_{\text{diag}} = \sum_{\alpha} |C_{\alpha}|^2 O_{\alpha\alpha}. \quad (14)$$

This exact result can be thought as the prediction of a ‘diagonal ensemble,’ where $|C_\alpha|^2$ is the weight of each state [26], and is different from any conventional ensemble of statistical mechanics.

3.1 Integrable Case with $V = J' = V' = 0$

Here, our set up is close in spirit to that of the experiment [8]. The initial state is the ground state of a harmonic trap with a staggered potential and, at $t = 0$, we turn off the staggered potential and allow the system to evolve in the presence of the trap [12]. In addition to density profiles and $n(k)$, we also study the occupation of the natural orbitals, which are the eigenstates of the one-particle density matrix, determined by the eigenvalue equation $\sum_{k=1}^N \rho_{jk} \phi_k^n = \lambda_\eta \phi_j^n$. The lowest natural orbital is also the most highly occupied.

Figure 1 depicts the evolution of the occupation of the zero-momentum state $n(k = 0)$ and the lowest natural orbital λ_0 when, (i) the initial state has a half-filled insulator in the center of the trap [Fig. 2(a)] and, (ii) two insulating shoulders surround a central superfluid region [Fig. 2(d)]. In both cases, the two observables undergo relaxation dynamics, which ultimately brings them to an almost time-independent result. This shows that relaxation is not precluded by integrability, and the question that remains to be answered is how to describe these observables after relaxation. As seen in Fig. 1, they are clearly different from the predictions of the grand-canonical ensemble (GE in the figures), which are obtained after determining the temperature and chemical potential so that

$$E = \frac{1}{Z} \text{Tr} \left\{ \hat{H} e^{-(\hat{H} - \mu \hat{N})/k_B T} \right\}, \quad N = \frac{1}{Z} \text{Tr} \left\{ \hat{N} e^{-(\hat{H} - \mu \hat{N})/k_B T} \right\}, \quad (15)$$

where $\hat{N} = \sum_j \hat{b}_j^\dagger \hat{b}_j$, and E and N are the average energy and particle number in the time evolving state, which are conserved during the evolution. We note that for the system sizes considered, finite size effects are negligible.

The lack of relaxation to the thermal state may not be surprising considering that the system is integrable, and, hence, the existence of conserved quantities may preclude thermalization. In Ref. [10], a generalization of the Gibbs ensemble (GGE) was proposed in order to account for the conserved quantities and still be able to statistically describe integrable systems. The density matrix for the GGE was determined by maximizing the many-body Gibbs entropy $S = k_B \text{Tr} [\hat{\rho}_c \ln(1/\hat{\rho}_c)]$ subject to the constraints imposed by all the integrals of

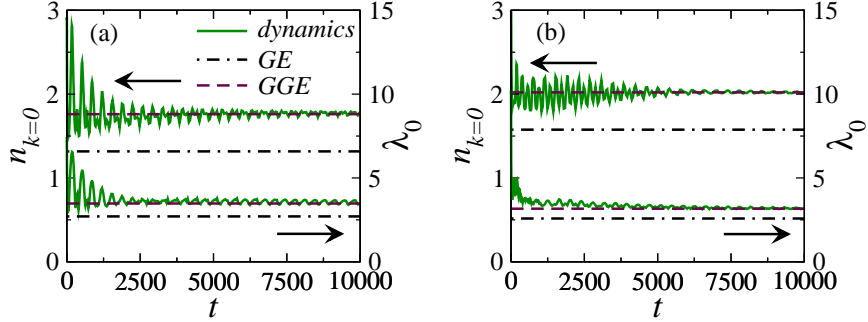


Figure 1: Dynamics of $n(k = 0)$ (top plots) and λ_0 (bottom plots) after a staggered potential is turned off in harmonically confined systems with 900 lattice sites and a trap curvature $V_2 = 3 \times 10^{-5}J$. t is given in units of \hbar/J , and the evolution starts from the ground state in the presence of a staggered potential of strength $0.5J$. The number of particles is: (a) $N = 200$ and (b) $N = 299$. [The corresponding initial density profiles can be seen in Figs. 2(a) and 2(d)]. The dashed-dotted lines depict the results within the grand-canonical ensemble (GE), with (a) $T = 0.31J$ and (b) $T = 0.33J$, and the dashed lines the results within the generalized Gibbs ensemble (GGE).

motion. The result reads

$$\hat{\rho}_c = \frac{1}{Z_c} e^{-\sum_{j=1}^L \lambda_j \hat{I}_j}, \quad Z_c = \text{Tr} \left\{ e^{-\sum_{j=1}^L \lambda_j \hat{I}_j} \right\} \quad (16)$$

where Z_c is the generalized partition function, $\{\hat{I}_j\}$ is a full set of integrals of motion, and $\{\lambda_j\}$ are the Lagrange multipliers. The Lagrange multipliers are computed using the expectation values of the full set of integrals of motion in the initial state, i.e., $\langle \hat{I}_j \rangle_{\text{ini}} = \text{Tr} \{ \hat{I}_j \hat{\rho}_c \}$. For HCBs, which can be mapped to noninteracting fermions, a natural set of integrals of motion is provided by the projection operators to the noninteracting single particle eigenstates $\{\hat{I}_j\} = \{\hat{\gamma}_j^{f\dagger} \hat{\gamma}_j^f\}$, where $\{\hat{\gamma}_j^{f\dagger}\}$ ($\{\hat{\gamma}_j^f\}$) creates (annihilates) a single particle in an eigenstate of Eq. (4). The resulting Lagrange multipliers read $\lambda_j = \ln[(1 - \langle \hat{I}_j \rangle_{\text{ini}}) / \langle \hat{I}_j \rangle_{\text{ini}}]$. They allow one to build the density matrix in Eq. (16) and to compute expectation values as was described for the grand-canonical ensemble in Sec. 2.1.

Figure 1 shows that the GGE calculations for $n(k = 0)$ and λ_0 properly predict the outcome of the relaxation dynamics. We have also computed the time average (between $t = 5000\hbar/J$ and $10000\hbar/J$) of the full density profiles, $n(k)$, and λ_η . They are shown in Fig. 2. There, the time averages are compared with the

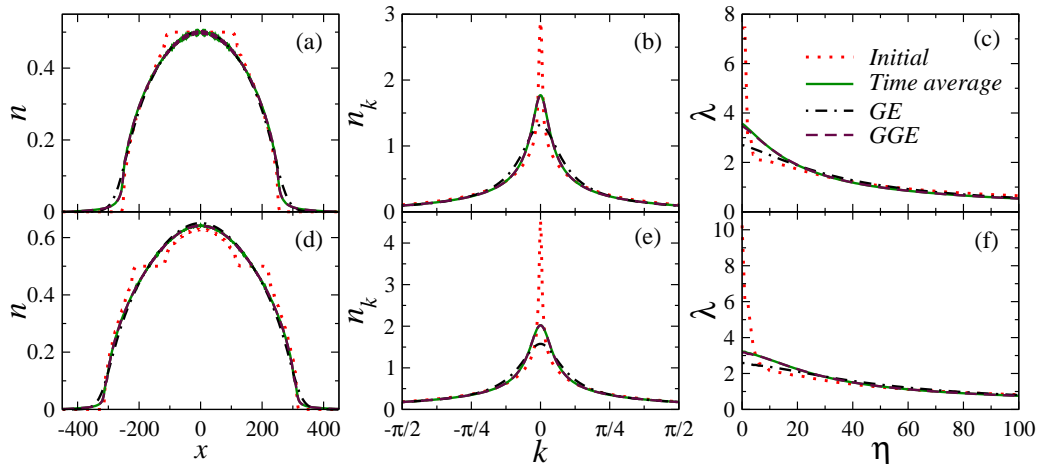


Figure 2: Initial state and time average values of: (a),(d) density profiles, (b),(e) momentum distribution functions, and (c),(f) occupation of the lowest 100 natural orbitals. The averages are computed between $t = 5000\hbar/J$ and $t = 10000\hbar/J$ with measurements done in time intervals $\Delta t = 40\hbar/J$, and correspond to the dynamics depicted in Fig. 1. The results of the time average are compared with those obtained in the grand-canonical ensemble (GE) and the generalized Gibbs ensemble (GGE) described in the text. The number of particles is $N = 200$ (a)–(c) and $N = 299$ (d)–(f). In (a) and (d), for the initial state, the occupations plotted are the averaged density per unit cell. Note that in the presence of the staggered potential, the density exhibits large fluctuations from site to site. Flat regions of the unit cell occupations correspond to insulating domains [12].

results for the initial state and with the predictions of the GE and the GGE. That comparison clearly shows that, unlike the GE, the GGE is able to predict all those single particle observables after relaxation. Note that, when written in the bosonic language, the constraints lose the bilinear character they have in the fermionic representation, i.e., the outcome of the GGE calculation is not at all trivial, as it would be if done for noninteracting fermions. Recent numerical and analytical studies have addressed various aspects of the GGE [10, 11, 12, 13, 14, 15, 16, 19], while a microscopic understanding for the agreement between the predictions of the GGE and the diagonal ensemble was presented in Ref. [23].

3.2 Nonintegrable Case with $V^{\text{ext}} = 0$

To study the effects of breaking integrability, we prepare an initial state that is an eigenstate of a Hamiltonian (in the total momentum $k = 0$ sector) with $J_{\text{ini}}, V_{\text{ini}}, J', V'$ and then quench the nearest-neighbor parameters to $J_{\text{fin}}, V_{\text{fin}}$ without changing J', V' . The same quench is repeated for different values of J', V' as one departs from $J' = V' = 0$ [31]. To find whether the dynamics brings the observables to the predictions of the diagonal ensemble (14), we calculate the normalized area between the observables during the time evolution and their infinite time average, i.e., $\delta n_k(t) = (\sum_k |n(k, t) - n_{\text{diag}}(k)|) / \sum_k n_{\text{diag}}(k)$. Similarly, we compute δN_k for the structure factor $N(k)$, which is the Fourier transform of the density-density correlations.

In Fig. 3, we show results for δn_k and δN_k vs t for three different quenches and two system sizes. The time evolution is very similar in all cases, and is consistent with a fast relaxation of both observables towards the diagonal ensemble prediction (in a time scale $t \sim \hbar/J$). The average differences after relaxation and their fluctuations can be seen to decrease with increasing system size. From these results, we infer that, for very large systems sizes, $n(k)$ and $N(k)$ should in general

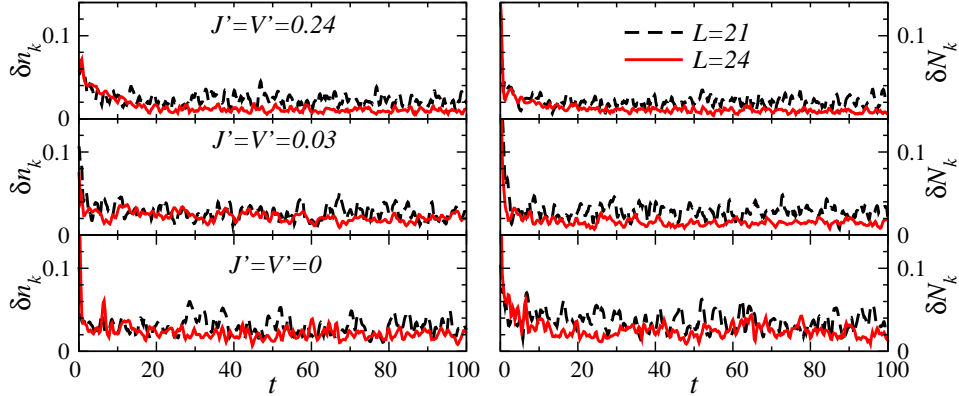


Figure 3: Evolution of δn_k (left panels) and δN_k (right panels) after a quench from $J_{\text{ini}} = 0.5J, V_{\text{ini}} = 2.0J$ to $J_{\text{fin}} = J, V_{\text{fin}} = J$, with $J'_{\text{ini}} = J'_{\text{fin}} = J'$ and $V'_{\text{ini}} = V'_{\text{fin}} = V'$, for two system sizes. The initial state was selected within the eigenstates with total momentum $k = 0$ such that after the quench the effective temperature is $T = 3.0$ in all cases. Given the energy of the initial state E , T follows from $E = Z^{-1} \text{Tr}\{\hat{H} e^{-\hat{H}/k_B T}\}$, where $Z = \text{Tr}\{e^{-\hat{H}/k_B T}\}$. The trace runs over the full spectrum.

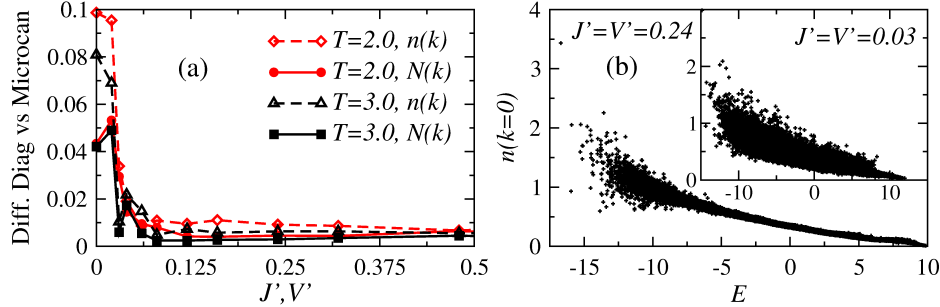


Figure 4: (a) Differences between the predictions of the diagonal and microcanonical ensembles (calculated as δn_k and δN_k in Fig. 3). Results are shown for $T = 2.0$ and $T = 3.0$. (b) $n(k = 0)$ as a function of the energy for all the eigenstates of the Hamiltonian (including all momentum sectors). (main panel) $J = V = 1$ and $J' = V' = 0.24$. (inset) $J = V = 1$ and $J' = V' = 0.03$. The systems in (a) and (b) have $L = 24$ and $N_b = 8$.

relax to exactly the predictions of Eq. (14) even if the system is very close or at integrability.

We then say that thermalization takes place if the results of conventional statistical ensembles and those of the diagonal ensemble are the same. In Fig. 4(a), we compare the diagonal ensemble results with the predictions of the microcanonical ensemble for our two observables of interest. Far from integrability the differences are small and decrease with increasing system size [31], i.e., thermalization takes place. As one approaches integrability, the differences increase, signaling a breakdown of thermalization in 1d.

Thermalization away from integrability, as well as its failure close to integrability, can be understood in terms of the eigenstate thermalization hypothesis (ETH) [26, 38, 39]. ETH states that, for generic systems, the fluctuations of eigenstate expectation values of observables is small between eigenstates that are close in energy, which implies that the microcanonical average is identical to the prediction of each eigenstate, which is the same as saying that the eigenstates already exhibit thermal behavior. If this holds, thermalization in an isolated quantum system will follow for any distribution of $|C_\alpha|^2$ that is narrow enough in energy.

The main panel in Fig. 4(b) depicts $n(k = 0)$ [similar results were obtained for $n(k \neq 0)$ and $N(k)$] in each eigenstate of the Hamiltonian when the system is far from integrability. After a region of low energies where the eigenstate expectation values exhibit large fluctuations, one can see another region where fluctuations are

small (presumably vanishing in the thermodynamic limit) and ETH holds. The inset shows that for a system close to the integrable point, in which thermalization is absent [Fig. 4(a)], the eigenstate-to-eigenstate fluctuations of $n(k=0)$ are very large over the entire spectrum (they do not vanish in the thermodynamic limit) and ETH does not hold.

Acknowledgments

This work was supported by the Office of Naval Research. We thank V. Dunjko, A. Muramatsu, M. Olshanii, and L. F. Santos for discussions.

References

- [1] G. Gallavotti, *Statistical Mechanics: A Short Treatise* (Springer, Berlin, 1999).
- [2] E. Fermi, J. Pasta, and S. Ulam, Los Alamos Report , LA (1955).
- [3] D. K. Campbell, P. Rosenau, and G. M. Zaslavsky, *Chaos* **15**, 015101 (2005).
- [4] M. Rasetti, *Modern Methods in Equilibrium Statistical Mechanics* (World Scientific, Singapore, 1986).
- [5] T. Kinoshita, T. Wenger, and D. S. Weiss, *Science* **305**, 1125 (2004).
- [6] B. Paredes, A. Widera, V. Murg, O. Mandel, S. Fölling, I. Cirac, G. V. Shlyapnikov, T. W. Hänsch, and I. Bloch, *Nature* **429**, 277 (2004).
- [7] T. Kinoshita, T. Wenger, and D. S. Weiss, *Phys. Rev. Lett.* **95**, 190406 (2005).
- [8] T. Kinoshita, T. Wenger, and D. S. Weiss, *Nature* **440**, 900 (2006).
- [9] S. Hofferberth, I. Lesanovsky, B. Fischer, T. Schumm, and J. Schmiedmayer, *Nature* **449**, 324 (2007).
- [10] M. Rigol, V. Dunjko, V. Yurovsky, and M. Olshanii, *Phys. Rev. Lett.* **98**, 050405 (2007).
- [11] M. A. Cazalilla, *Phys. Rev. Lett.* **97**, 156403 (2006).

- [12] M. Rigol, A. Muramatsu, and M. Olshanii, Phys. Rev. A **74**, 053616 (2006).
- [13] P. Calabrese and J. Cardy, J. Stat. Mech. , P06008 (2007).
- [14] M. Cramer, C. M. Dawson, J. Eisert, and T. J. Osborne, Phys. Rev. Lett. **100**, 030602 (2008).
- [15] T. Barthel and U. Schollwöck, Phys. Rev. Lett. **100**, 100601 (2008).
- [16] M. Kollar and M. Eckstein, Phys. Rev. A **78**, 013626 (2008).
- [17] A. Flesch, M. Cramer, I. P. McCulloch, U. Schollwöck, and J. Eisert, Phys. Rev. A **78**, 033608 (2008).
- [18] D. Rossini, A. Silva, G. Mussardo, and G. E. Santoro, Phys. Rev. Lett. **102**, 127204 (2009).
- [19] A. Iucci and M. A. Cazalilla, Phys. Rev. A **80**, 063619 (2009).
- [20] J. Mossel and J.-S. Caux, New J. Phys. **12**, 055028 (2010).
- [21] P. Barmettler, M. Punk, V. Gritsev, E. Demler, and E. Altman, New J. Phys. **12**, 055017 (2010).
- [22] D. Fioretto and G. Mussardo, New J. Phys. **12**, 055015 (2010).
- [23] A. C. Cassidy, C. W. Clark, and M. Rigol, Phys. Rev. Lett. **106**, 140405 (2011).
- [24] C. Kollath, A. M. Läuchli, and E. Altman, Phys. Rev. Lett. **98**, 180601 (2007).
- [25] S. R. Manmana, S. Wessel, R. M. Noack, and A. Muramatsu, Phys. Rev. Lett. **98**, 210405 (2007).
- [26] M. Rigol, V. Dunjko, and M. Olshanii, Nature **452**, 854 (2008).
- [27] M. Moeckel and S. Kehrein, Phys. Rev. Lett. **100**, 175702 (2008).
- [28] P. Reimann, Phys. Rev. Lett. **101**, 190403 (2008).
- [29] G. Roux, Phys. Rev. A **79**, 021608 (2009).
- [30] M. Eckstein, M. Kollar, and P. Werner, Phys. Rev. Lett. **103**, 056403 (2009).

- [31] M. Rigol, Phys. Rev. Lett. **103**, 100403 (2009a).
- [32] M. Rigol, Phys. Rev. A **80**, 053607 (2009b).
- [33] M. Moeckel and S. Kehrein, Ann. Phys. **324**, 2146 (2009).
- [34] L. F. Santos and M. Rigol, Phys. Rev. E **81**, 036206 (2010).
- [35] G. Roux, Phys. Rev. A **81**, 053604 (2010).
- [36] P. Reimann, New J. Phys. **12**, 055027 (2010).
- [37] M. Rigol and L. F. Santos, Phys. Rev. A **82**, 011604(R) (2010).
- [38] J. M. Deutsch, Phys. Rev. A **43**, 2046 (1991).
- [39] M. Srednicki, Phys. Rev. E **50**, 888 (1994).
- [40] E. Lieb, T. Shultz, and D. Mattis, Ann. Phys. (NY) **16**, 406 (1961).
- [41] T. Holstein and H. Primakoff, Phys. Rev. **58**, 1098 (1940).
- [42] P. Jordan and E. Wigner, Z. Phys. **47**, 631 (1928).
- [43] M. Rigol and A. Muramatsu, Phys. Rev. A **72**, 013604 (2005a).
- [44] M. Rigol and A. Muramatsu, Mod. Phys. Lett. **19**, 861 (2005b).
- [45] M. Rigol, Phys. Rev. A **72**, 063607 (2005).
- [46] W. H. Press, S. A. Teukolsky, W. T. Vetterling, and B. P. Flannery, *Numerical Recipes: The Art of Scientific Computing, Third Edition* (Cambridge University Press, Cambridge, 2007).